Applied Catalysis B: Environmental 339 (2023) 123097

Contents lists available at ScienceDirect

Applied Catalysis B: Environmental

journal homepage: www.elsevier.com/locate/apcatb

Fabrication of ZnO/CuO nanoforests and their applicability to microbial photoelectrochemical cells

Ryosuke Matsuo [a], Yuki Takahashi [b], Seiichi Watanabe [c], Satoshi Okabe [d,*]

[a] Department of Environmental Engineering, Graduate School of Engineering, Hokkaido University, North-13, West-8, Kita-ku, Sapporo, Hokkaido 0608628, Japan
[b] Department of Engineering, Graduate School of Engineering, Hokkaido University, North-13, West-8, Kita-ku, Sapporo, Hokkaido 0608628, Japan
[c] Department of Engineering, Faculty of Engineering, Hokkaido University, North-13, West-8, Kita-ku, Sapporo, Hokkaido 0608628, Japan
[d] Department of Environmental Engineering, Faculty of Engineering, Hokkaido University, North-13, West-8, Kita-ku, Sapporo, Hokkaido 0608628, Japan

ARTICLE INFO

Keywords:
Photoelectrochemical hydrogen generation
ZnO/CuO nanoforests
Galvanic submerged photo-synthesis
Semi-artificial photosynthesis
Environmental applicability

ABSTRACT

Three-dimensional ZnO/CuO nanoforests (NFRs) were fabricated via the galvanic submerged photosynthesis of crystallites in water at ambient temperature and pressure, and their photoelectrochemical (PEC) properties and applicability to microbial PEC (MPEC) cells were evaluated. ZnO/CuO NFRs irradiated with UV light for 48 h showed a high PEC current of -2.9 ± 1.3 mA/cm^2 and hydrogen (H_2) generation rate of 0.63 ± 0.29 μmol/cm^2/day at 0 V vs. RHE owing to their superior light absorption, large BET specific surface area, and low charge recombination. The biocompatibility of the ZnO/CuO NFRs was evaluated by assessing their influence on *Escherichia coli* MG1655 growth. The ZnO/CuO NFRs leached Cu^{2+} and inhibited bacterial growth after immersion in the medium. Cu elution could be prevented by maintaining the potential at 0.01 V vs. RHE. The ZnO/CuO NFRs can be used as photocathodes for PEC H_2 generation and the MPEC-based synthesis of valuable CO_2-reduction products.

1. Introduction

Semiartificial photosynthesis is a promising emerging technology that can convert solar energy into valuable fuels or chemicals. In particular, hybrid inorganic–biological photosynthesis systems provide an opportunity to overcome the limitations of natural and artificial photosynthesis. Inorganic biological systems utilize synthetic materials, such as semiconductors, as light absorbers (i.e., photoanodes or photocathodes) and microbial cells as catalysts. In microbial hybrid systems, complex compounds that are not feasible in purely artificial systems can be produced by utilizing microbial metabolic pathways, and the self-replicating nature of microorganisms leads to high scalability and selectivity [1,2]. However, the volumetric production rates in such systems are inherently low owing to low microorganism–electrode charge transfer; thus, further improvements are necessary.

Metal-oxide semiconductors have attracted considerable attention because of their high chemical stability and low cost [3]. However, metal-oxide semiconductors exhibit limited light absorption, which hinders their practical applications [4]. Because 3D nanomaterials, such as hierarchical nanostructures and branched nanowires (NWs), have a large specific surface area, they demonstrate improved light absorption, prevent charge recombination [5–8], and possess excellent gas evolution kinetics [9]. The use of 3D nanostructures is a promising strategy to obtain efficient photoelectrochemical (PEC) water splitting. Heterostructures of *p*- and *n*-type metal oxide semiconductors are also promising options. A *p*-*n* heterojunction could improve photogenerated charge separation and light absorption [6,10–13].

The applications of zinc oxide (ZnO) and copper oxide (CuO) have sparked great interest because these materials are inexpensive, abundant, and highly tailorable; they also exhibit outstanding electrical and optical properties [14–17]. The 3D ZnO/CuO nanoheterostructure has a high specific surface area and *p*-*n* junction between *p*-CuO and *n*-ZnO,

Abbreviations: NFRs, nanoforests; G-SPSC, galvanic submerged photosynthesis of crystallites; MPEC, microbial photoelectrochemical; ICPE, inductively coupled plasma emission spectroscopy; ZnO, zinc oxide; CuO, copper oxide; NP, nanoparticle; SPSC, submerged photosynthesis of crystallites; NWs, nanowires; RF, radio-frequency; NR, nanorod; WE, working electrode; CE, counter electrode; RE, reference electrode; LSV, linear sweep voltammetry; FE-SEM, field-emission scanning electron microscopy; XPS, X-ray photoelectron spectroscopy; XRD, X-ray diffraction; BET, Brunauer–Emmett–Teller; ABPE, applied bias photon-to-current efficiency; DMSO, dimethyl sulfoxide; EIS, electrochemical impedance spectroscopy; PBS, phosphate-buffered saline.

* Corresponding author.
E-mail address: sokabe@eng.hokudai.ac.jp (S. Okabe).

https://doi.org/10.1016/j.apcatb.2023.123097
Received 26 May 2023; Received in revised form 10 July 2023; Accepted 13 July 2023
Available online 20 July 2023

leading to improved light absorption and low charge recombination [5, 18–21]. Therefore, this material is considered suitable for a wide range of practical applications, such as sensors [22–24], photocatalysts [18, 21,25–28], and photoelectrodes [5,8,19,20,29,30]. ZnO/CuO heterojunction branched NWs show promise for PEC hydrogen (H_2) generation [8]. ZnO/CuO composites are generally fabricated by complex methods, such as hydrothermal growth [5,8,18,31], thermal oxidation [19,20], and the sol-gel method [26]. Furthermore, radio-frequency (RF) magnetron sputtering that requires high vacuum pressure was used to provide a ZnO seeding layer [6,8,11]. Thus, these fabrication methods unfortunately require harsh conditions such as high temperatures and pressures, high/low-pH solutions, and complex procedures. Therefore, a simple, environmentally friendly, and feasible fabrication process is required.

The galvanic submerged photosynthesis of crystallites (G-SPSC), a novel environmentally friendly fabrication method of metal oxide nano heterostructures was recently proposed, in which metal oxides can be fabricated via galvanic contact reaction followed by UV light irradiation at ambient temperature and pressure in pure water [32,33]. In the case of Zn and Cu, galvanic contact induces Zn^{2+} dissolution and ZnO nanoparticle (NP) generation on Cu surface in pure water [32]. The submerged photosynthesis of crystallites (SPSC) induces the vertical growth of the ZnO NP seeds via photochemical reactions under UV irradiation [34,35]. ZnO/CuO nanoforests (NFRs) with 3D nanostructures were recently successfully fabricated via G-SPSC [36]. However, the following three issues have yet to be addressed. First, the fabrication conditions of 3D ZnO/CuO NFRs have not been optimized. In the G-SPSC process, RF magnetron sputtering was still used to provide ZnO seeding layers to facilitate the formation of ZnO NFRs [36], which makes this process more labor-intensive, costly and less environmentally friendly. Second, information on the PEC properties and performance of the fabricated 3D ZnO/CuO NFRs, especially PEC current and H_2 production, have not been measured to date. Third, the applicability of ZnO/CuO NFRs as photocathodes for semi-artificial photosynthesis has not been evaluated. These issues must be resolved for the improvement of their PEC performance and consequently practical applications.

Therefore, the present study expounds on these issues for the first time. Herein, ZnO/CuO NFRs were fabricated using the G-SPSC method at ambient temperature and pressure in pure water. The effects of the fabrication conditions (i.e., presence/absence of ZnO sputter deposition and different UV irradiation times) on the physicochemical and PEC properties (i.e., PEC current and H_2 generation ability) of the ZnO/CuO NFRs were investigated. The charge transfer resistance R_{ct} and toxicity of the ZnO/CuO NFRs to *Escherichia coli* MG1655 as a model microorganism were subsequently investigated to assess their practicability as a photocathode in semi-artificial photosynthesis.

2. Experimental

2.1. Fabrication of the ZnO/CuO NFRs

CuO NWs were synthesized via thermal oxidation on a Cu mesh (Φ = 80 μm, #120 μm) [37]. Before thermal oxidation, the Cu meshes were cleaned as follows. First, the Cu meshes were immersed in 1 M KOH (pH 14) for 10 min, rinsed with pure water, and cleaned with pure water for 5 min using an ultrasonic washer. The samples were dried with paper and transferred to an electric furnace (KDF-S70, Denken-Highdental Co., Ltd., Japan) for annealing at 500 °C for 4 h. The annealing temperature was increased from the room temperature up to 500 °C within 10 min. The annealing temperature was set to 500 °C because denser and thicker NW structures are generated at this temperature than at 400 and 600 °C [36]. The samples were then cooled to room temperature in a furnace.

The CuO NW meshes were transferred to an RF magnetron sputtering machine (JEC-SP360R, JEOL, Japan) and coated with a ZnO seeding layer for ZnO nanorod (NR) growth. A ZnO target was used for sputtering, which was performed for 1 h at 1 Pa under an Ar atmosphere.

The ZnO NRs were synthesized on the surface of CuO NWs using the G-SPSC method, which can be performed at room temperature and pressure by UV irradiation of the samples in pure water [32]. For galvanic contact, Zn foil (99.99% pure, 0.05 × 100 × 200 mm, Nilaco, Japan) was placed under the CuO mesh. The samples were immersed in pure water and irradiated with UV light for 24 – 48 h behind a dark curtain using a UV light source (B-100AP, UVP, USA) at a wavelength of 365 nm to synthesize ZnO NRs on the surface of the CuO NWs. A Cu wire was spot-welded to one side of the synthesized ZnO/CuO mesh, and the four sides were coated with epoxy to prevent the exposure of Cu to the electrolyte.

For convenience, the ZnO/CuO samples were denoted *S*-UV*T* and UV*T*, where *S* and *T* indicate the presence of sputtering and UV irradiation time, respectively. For example, S-UV24 refers to the sample prepared with 24 h of UV irradiation and sputter deposition, while UV48 refers to the sample prepared with 48 h of UV irradiation without sputter deposition.

2.2. Physical and chemical properties

The surface structure of the fabricated ZnO/CuO NFRs was observed using field-emission scanning electron microscopy (FE-SEM, JSM-7001FA, JEOL, Japan). To identify the structural component as well as lattice strain of ZnO/CuO NFRs, X-ray diffraction (XRD) profiles were collected by MiniFlex600 (Rigaku, Japan). Peak fitting was performed with ICDD numbers 01–071–3830, 01–089–5898, 01–071–4310, and 00–001–1241 as references for ZnO, CuO, Cu_2O, and Cu, respectively. The binding states of the atoms on the surfaces of the samples were observed using X-ray photoelectron spectroscopy (XPS, JPS-9200, JEOL, Japan). XPS was conducted with an Al Kα source at 1486.6 eV, with a voltage of 10 kV and an emission current of 10 mA with charge neutralization at 1.5 eV and 6.0 A. Absorbance spectra were recorded using a UV–vis spectrophotometer (V-770, Jasco, Japan).

The specific surface areas of the samples were determined using the Brunauer–Emmett–Teller (BET) method in liquid nitrogen (N_2) at a temperature of 77 K using a sorption (surface area and pore size) analyzer (Autosorb 6AG, Yuasa Ionics, Japan). Prior to the BET specific surface area measurements, the samples were cut into small pieces and evacuated at 150 °C for 2 h to remove impurities and gases from their surface. The data obtained from the BET plots had a correlation coefficient of 0.9 or higher.

2.3. PEC performance of the ZnO/CuO NFRs

The PEC current density and H_2 production rate were measured using a three-electrode system with the sample as the working electrode (WE), Pt wire (10 cm) as the counter electrode (CE), and Ag/AgCl (E^0 = 195 mV vs. RHE at 25 °C, RE-1B, BAS, Japan) as the reference electrode (RE). The PEC cell was a dual-chamber reactor comprising a medium Pyrex glass bottle separated by a Nafion 117 proton exchange membrane (Sigma-Aldrich, USA). The electrolyte was a phosphate-buffered saline (PBS, pH 7.2) containing 0.25 M Na_2SO_4. The electrolyte was purged with N_2 gas for more than 20 min before the measurement. A potentiostat (ALS760E, BAS) was used for electrochemical measurements. Linear sweep voltammetry (LSV) was performed at a scan rate of 10 mV/s. Chronoamperometry was used to determine the H_2 production rate. The potentials of the WE were 0 and − 0.69 V vs. RHE. The current–time (*I*–*t*) curve was used to obtain the current density under intermittent light irradiation; the WE was maintained at 0.02 V vs. RHE, and light irradiation was conducted at 10 s intervals. Before LSV and the H_2 generation experiment at − 0.69 V vs. RHE, the ZnO/CuO NFRs were maintained at − 0.69 V vs. RHE for 10 min

A visible-light irradiator (LC8, L9588–04–03, Hamamatsu, Japan) with a Xe light source capable of emitting 400–700 nm rays was equipped with a filter to block wavelengths beyond 350–600 nm and placed 5 cm from the sample. An irradiation intensity of 100 mW/cm^2

was used for the *I–t* curve measurements under intermittent light irradiation and LSV; irradiation intensities of 230 and 100 mW/cm^2 were also used to determine the H_2 production rate at − 0.69 V vs. RHE and 0 V vs. RHE, respectively.

A H_2 needle sensor (H_2-N, Unisense, Denmark) was used to measure H_2 concentrations in the liquid phase. The tip of the needle sensor was immersed in the electrolyte in the cathode chamber, and the H_2 concentration in the liquid phase was measured over time.

2.4. Toxicity of the ZnO/CuO NFRs to Escherichia coli MG1655

E. coli MG1655 was inoculated from glycerol stock into LB medium (10 g/L tryptone, 5 g/L yeast extract, 10 g/L NaCl, pH 7.0) and incubated under aerobic conditions at 35 °C for 24 h with shaking. Thereafter, 2 mL of the culture was inoculated into the UV48 soaked culture medium, which was purged with N_2 gas for 1 h before inoculation, and incubated in an anaerobic chamber to measure the growth of the bacterium. The culture medium in the experimental system was composed of 250 mL of LB medium containing 1 g/L glucose and 0.5% (v/v) dimethyl sulfoxide (DMSO). The OD_{600} of *E. coli* MG1655 was measured using a UV–vis spectrophotometer (V-630Bio, Jasco, Japan).

The experimental systems included UV48 without poising potential (light/dark), UV48 with poising potential (light/dark at 0.01 V vs. RHE), and no electrode (*E. coli* MG1655) as a control system. Each experiment was performed in triplicate except for UV48 (dark at 0.01 V vs. RHE, n = 2). The systems were maintained at 0.01 V vs. RHE in a dual-chamber reactor consisting of a medium Pyrex glass bottle separated by a Nafion 117 proton exchange membrane (Sigma-Aldrich). The other experimental systems were conducted in a single-chamber PYREX glass reactor. Voltage was applied using a three-electrode system with a potentiostat (HA-151B, HOKUTO DENKO CORPORATION, Japan) and data logger (midi LOGGER GL220, GRAPHTEC Corporation, Japan) for current and potential measurements. The WE of the three-electrode system was UV48, the CE was graphite felt (2.5 × 4 cm^2) with stainless steel wire, and the RE was Ag/AgCl (E^0 = 0.199 V vs. NHE at 25 ℃, ICC. Japan). The light source was similar to that used in the PEC performance measurements and emitted rays with wavelengths ranging from 400 to 600 nm; this light source was placed 10 cm away from the sample. The light intensity was ~70 mW/cm^2.

2.5. Quantification of Zn and Cu concentrations

The ZnO/CuO NFRs were immersed in an abiotic LB medium containing 1 g/L glucose and 0.5% (v/v) DMSO, and the concentrations of Zn and Cu in the liquid phase were measured using inductively coupled plasma emission spectroscopy (ICPE-9000, Shimadzu Corporation, Japan) with and without voltage application and light irradiation. As a pretreatment, organic matter in the sample was decomposed by adding 4 mL of inverse aqua regia (nitric acid: hydrochloric acid = 3:1) to the samples, followed by heating at 105 °C for 2 h. Then, the sample volume was scaled up to 50 mL using pure water, and the Zn and Cu concentrations were measured using ICPE.

2.6. Electrochemical impedance spectroscopy (EIS)

EIS was performed using a borosilicate glass dual-chamber three-electrode system separated by a Nafion 117 membrane (Sigma-Aldrich). Nyquist plots were prepared from the EIS profiles to estimate R_{ct}. The three-electrode system consisted of graphite felt (4 × 2.5 cm^2) with stainless steel wire or UV48 as the WE, Pt wire (10 cm) as the CE, and Ag/AgCl as the RE. The EIS measurements were performed from 100 kHz to 10 mHz with an amplitude of 5 mV and a potential of 0.02 V vs. RHE. The electrolyte was gently stirred during the measurements. Both the anolyte and catholyte were composed of 0.25 M Na_2SO_4 dissolved in PBS and adjusted to pH 7.2. The anode and cathode were filled with 300 mL of the electrolyte, which was degassed with N_2 gas for at least 30 min before measurement.

The Nyquist plot measured by EIS was curve-fitted by complex nonlinear least-squares regression using pyZwx [38] to estimate various parameters, including R_{ct}. A multiple Randles circuit with Warburg diffusion was used as the equivalent circuit for parameter estimation. Because a double-Randles circuit was used, two values of R_{ct} (R_{ct1} and R_{ct2}) were obtained. In the case of graphite felt, R_{ct1} originated from the stainless steel wire and R_{ct2} originated from the graphite felt. In the case of the ZnO/CuO NFRs, R_{ct1} originated from CuO and R_{ct2} originated from ZnO. To obtain an accurate estimation of R_{ct2} for the ZnO/CuO NFRs, we ignored the diffusion impedance of the Nyquist plot during curve fitting.

2.7. Calculation

Faradaic efficiency, which refers to the ratio between the measured and theoretical amount of H_2 production calculated from the current density, was estimated using the following equation:

$$Faradaic \quad efficiency(\%) = n_{H2}/(Q/2F) \times 100 \tag{1}$$

where n_{H2}, Q, and F are the amount of H_2 generated, total Coulomb produced by the current, and the Faradaic constant, respectively.

To evaluate the PEC performance of the photocathodes, applied bias photon-to-current efficiency (ABPE), which refers to the solar-to-hydrogen conversion efficiency with externally applied bias, was calculated from the measured photocurrent using the following equation:

$$ABPE(\%) = \left[\frac{|j_{ph}| \times |V_b|}{P_{total}}\right] \times 100 \tag{2}$$

where j_{ph}, V_b, and P_{total} denote the photocurrent density, applied voltage, and energy flux of the light source, respectively.

RHE potential was calculated using the following equation:

$$E(V \quad vs.RHE) = E(V \quad vs.Ag/AgCl) + 0.199 + 0.059 \times pH. \tag{3}$$

To determine the stability of the ZnO/CuO NFRs, the remaining ratio of current density was calculated by the following equation:

$$Remaining \quad ratio \quad (\%) = (current \quad density)/(maximum \quad current \quad density) \times 100. \tag{4}$$

3. Results and discussion

3.1. Fabrication of the ZnO/CuO NFRs

FE-SEM observation revealed that a NW structure developed on the surface of the Cu mesh (Fig. 1A, B). The wide-scan XPS profiles of the samples revealed that the NWs were composed of CuO, Cu_2O, or Cu (Fig. 1C). The high-resolution Cu 2p XPS spectrum showed CuO-specific satellite peaks indicative of $2p_{1/2}$ at 953.8 eV and $2p_{3/2}$ at 933.5 eV (Fig. 1D). Therefore, CuO NWs were successfully synthesized on a Cu mesh by thermal oxidation at 500 °C for 4 h.

ZnO NFR-like structures as previously reported [36] were synthesized on CuO NWs under various fabrication conditions by G-SPSC (Fig. 2A–D). The ZnO NRs-like structures, which measured nearly 1.0 μm in length, were longer than the hydrothermally synthesized ZnO NRs described in previous research (ca. 200 nm) [8]. Because the processing time of G-SPSC (days) is longer than that of the hydrothermal growth method (minutes), this method could result in longer ZnO NRs. However, it is not clear from SEM observations alone whether ZnO/CuO NFRs are really formed and how different UV irradiation times affect their elemental structure. Therefore, the elemental compositions and chemical bonding states of the NRs were investigated using XPS. The wide-scan XPS spectra of S-UV24 and S-UV48 showed the presence of

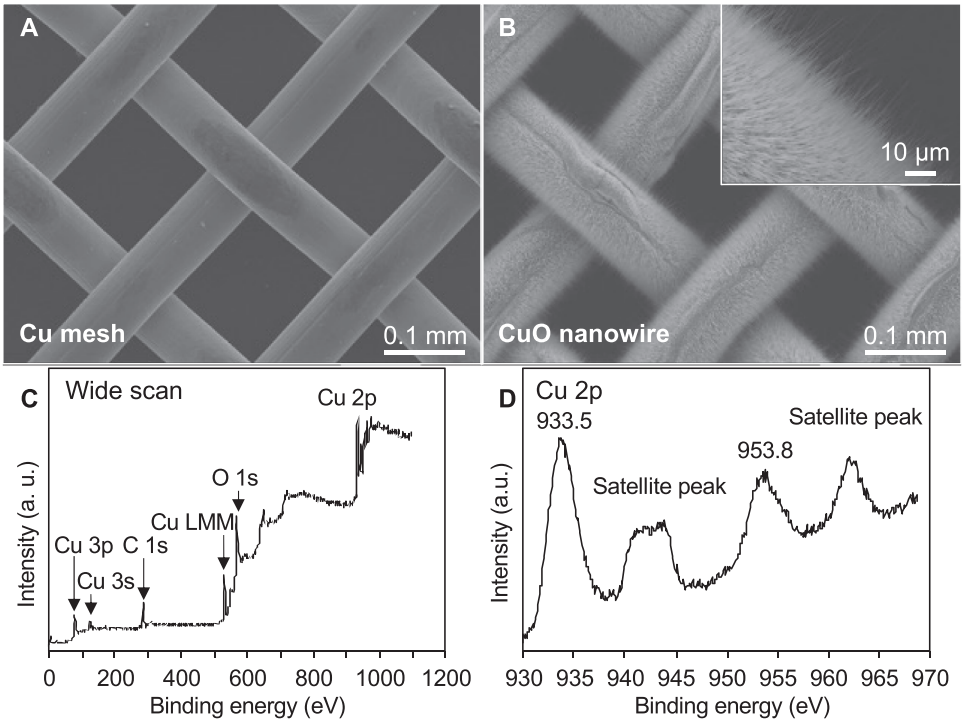

Fig. 1. FE-SEM images of (A) the Cu mesh and (B) CuO nanowire (NW) arrays grown on a Cu mesh by annealing at 500 °C for 4 h. (C) Wide-scan and (D) high-resolution Cu 2p XPS spectra of the CuO NW arrays after annealing at 500 °C for 4 h.

Zn, O, and C, with no Cu peaks (Fig. 2E), indicating that the NFR surface was covered with Zn compounds or Zn. However, the narrow-scan XPS profiles of UV24 and UV48 revealed the presence of Cu with a small satellite peak, indicating the presence of CuO (Fig. S1A, B). This is because sputtering provided a ZnO seeding layer for S-UV24 and S-UV48, which covered the CuO NWs completely, whereas ZnO NRs directly attached to the CuO NWs without sputtering. The type of Zn compounds in the samples was further identified by calculating the sum of the peak positions of Zn $2p_{3/2}$ and the Auger peak (Zn LMN) obtained by high-resolution XPS. The peak of Zn $2p_{3/2}$ was observed at 1022.0–1022.2 eV for all four samples (Fig. 2F), and its sum with the Auger peak was almost 2010 eV (Table 1). These findings indicate that the Zn compound was ZnO. Furthermore, XRD profile analysis confirms the formation of ZnO (Fig. S2A-D). UV48 and S-UV48 exhibited the strongest peaks at 35.34°and 35.54°, respectively (Fig. S2B, D), indicating that the well-developed heterostructure interfaces between (101) of ZnO and (−111) of CuO were created by48h UV irradiation. Thus, ZnO/CuO NFRs were successfully synthesized under all G-SPSC fabrication conditions employed in this study.

3.2. Physical and chemical properties of the ZnO/CuO NFRs

The UV–visible light absorption spectra for the ZnO/CuO NFRs fabricated under four different G-SPSC conditions were obtained (Fig. 3). High absorbance (>90%) was observed below 400 nm, whereas moderate absorbance (60–70%) was observed in the range of 400–600 nm. Compared with the other samples, UV48 exhibited higher absorbance in the visible light range (400–600 nm), likely because of the enhanced surface area of its dense and elongated structure, which induces the absorption of reflected light. According to the theoretical equation (bandgap = 1240 / λ (nm)), the adsorption wavelength of ZnO is less than 370 nm because the bandgap of ZnO is 3.37 eV. This finding indicates that the absorption wavelength of the ZnO/CuO NFRs was significantly improved by the formation of an interface dipole in their *p-n* type heterojunction [36].

The BET specific surface area of the ZnO/CuO NFRs was measured to evaluate the effect of the fabrication conditions (i.e., ZnO sputter deposition and UV irradiation time) (Fig. 4). The specific surface area of UV48 (2.23 ± 0.87 m^2/g) was comparable with that of S-UV48 but 1.4–1.8 times larger than those of UV24 and S-UV24. This result indicates that the specific surface area of the ZnO/CuO NFRs is dependent on the UV irradiation time but not on whether ZnO sputter deposition was conducted. A longer UV irradiation time results in longer ZnO NRs formed by SPSC [39]. This result suggests that an initial ZnO seed layer provided by sputtering at 1 Pa for 60 min is not necessary and that galvanic contact between the Zn foil and CuO mesh provides a sufficient number of ZnO seeds for NR growth. However, the CuO NWs were occasionally distorted by heat during the annealing process, resulting in large variations in the density and size of the ZnO NRs and, consequently, the specific surface area (i.e., standard deviations) of the obtained samples.

3.3. Photocurrent generation of the ZnO/CuO NFRs

LSV measurements were conducted to evaluate the PEC performance of the fabricated ZnO/CuO NFRs. UV48 yielded a maximum photocurrent density of -2.9 ± 1.3 mA/cm^2 at 0 V vs. RHE, which was 1.6–2.6 times higher than that obtained from samples fabricated under other conditions (Fig. 5A). The photocurrent density–time (*J–t*) curves were measured at 0.02 V vs. RHE under intermittent light irradiation to study the charge recombination of the ZnO/CuO NFRs (Fig. 5B). All fabricated ZnO/CuO NFRs exhibited excellent responses to light irradiation. However, sharp drops in the photocurrent spikes were observed during the light irradiation of S-UV24 and S-UV48, whereas UV24 and UV48 exhibited a more rectangular-shaped photocurrent response. These findings indicate the occurrence of charge recombination at the electrode/electrolyte interface of S-UV24 and S-UV48 [8,9,11,40]. Thicker ZnO NRs may have been generated by the deposition of the ZnO seed layer (by ZnO sputtering), during which charge recombination is more likely to occur owing to the larger distance between the photogenerated electrons and NR surface [7]. Therefore, the high photocurrent generation of UV48 may be attributed to its high light absorption, large BET

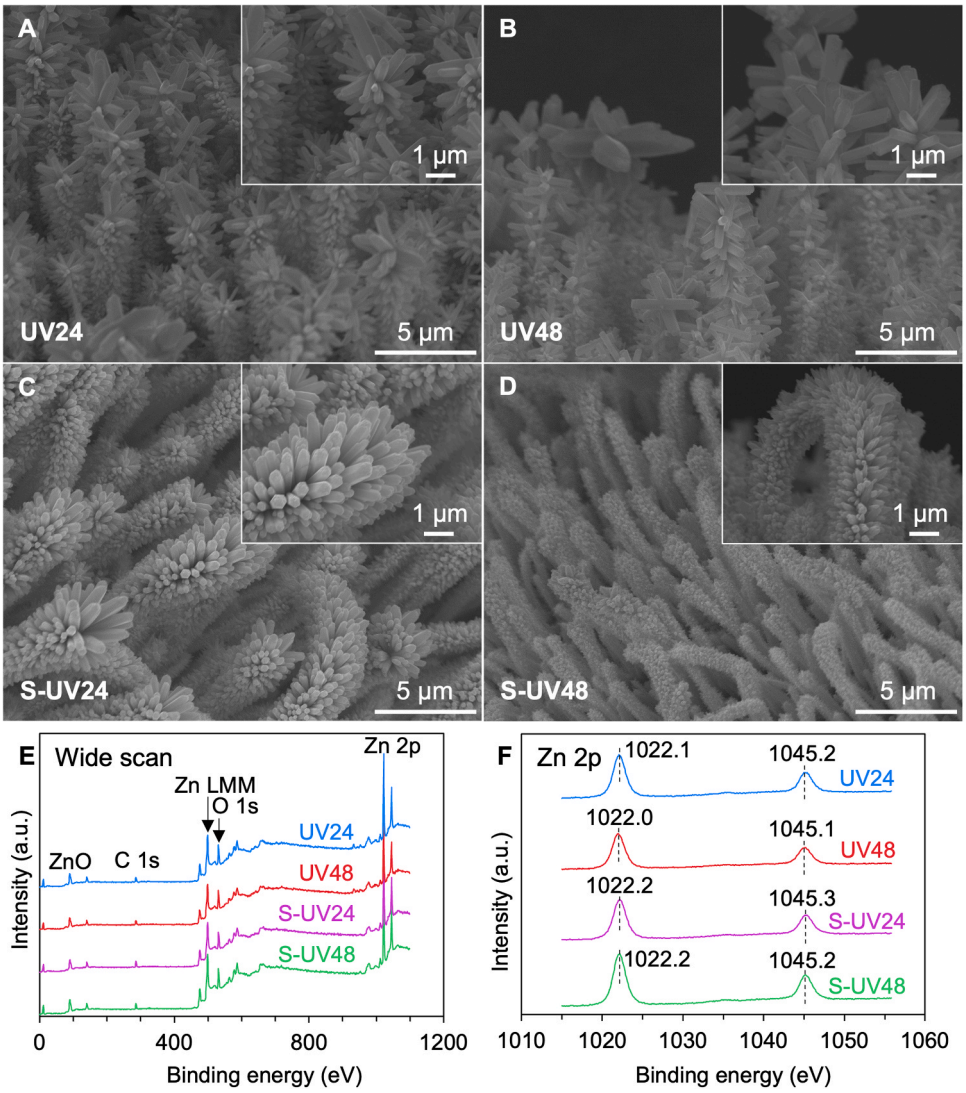

Fig. 2. FE-SEM images of ZnO nanorods (NRs) on the CuO NW arrays generated by UV irradiation for 24 h (A and C) and 48 h (B and D) in pure water with and without ZnO sputter deposition, respectively. (E) Wide-scan and (F) high-resolution Zn 2p XPS spectra of the ZnO/CuO NFR arrays.

Table 1
Peak positions in the Zn $2p_{3/2}$ and LMN spectra of the nanostructured ZnO/CuO composite.

	Zn $2p_{3/2}$ (eV)	Zn LMN (eV)	Total (eV)
UV24	1022.1	987.8	2009.9
UV48	1022.0	988.0	2010.0
S-UV24	1022.2	987.8	2010.0
S-UV48	1022.2	987.8	2010.0

specific surface area, and low charge recombination.

ABPE was calculated from the measured photocurrent density to evaluate the PEC performance of the photocathodes. The ZnO/CuO NFRs obtained without sputtering (i.e., UV48 and UV24) achieved higher ABPEs (0.67–0.70%) at 0.40 V vs. RHE than the other ZnO/CuO composites owing to the combined effects of high light absorption, large specific surface area, and low charge recombination (Fig. 5C). These results suggest the RF magnetron sputtering of ZnO, an energy- and time-consuming complicated process, is not necessary because it does not improve the performance of the photoelectrodes under the present conditions. The ABPE values obtained in this study were either higher than those of ZnO- and CuO-based materials [30,41] or similar to those of nanostructured materials, such as branched TiO_2 nanorods [7].

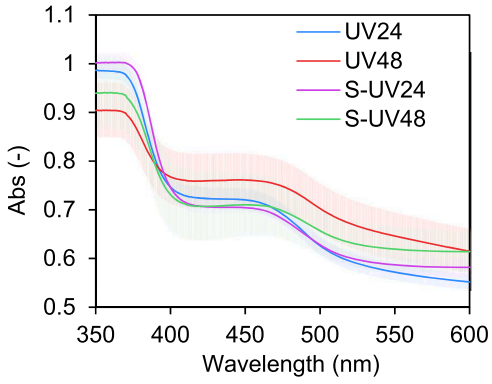

Fig. 3. UV–visible absorption spectra of the ZnO/CuO NFRs.

UV48 produced photocurrent densities that were over three times higher than those of previously reported ZnO/CuO composites (Table 2). Such excellent photocurrent generation ability can be attributed to the large specific surface area of the sample resulting from the formation of longer ZnO NRs. These results indicate that G-SPSC can be used to synthesize high-performance ZnO/CuO NFRs with low environmental

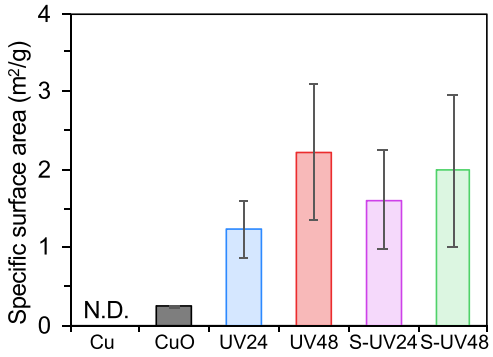

Fig. 4. BET specific surface area of the Cu mesh, CuO NW arrays, UV24, UV48, S-UV24, and S-UV48 detected using N_2 adsorption–desorption measurements.

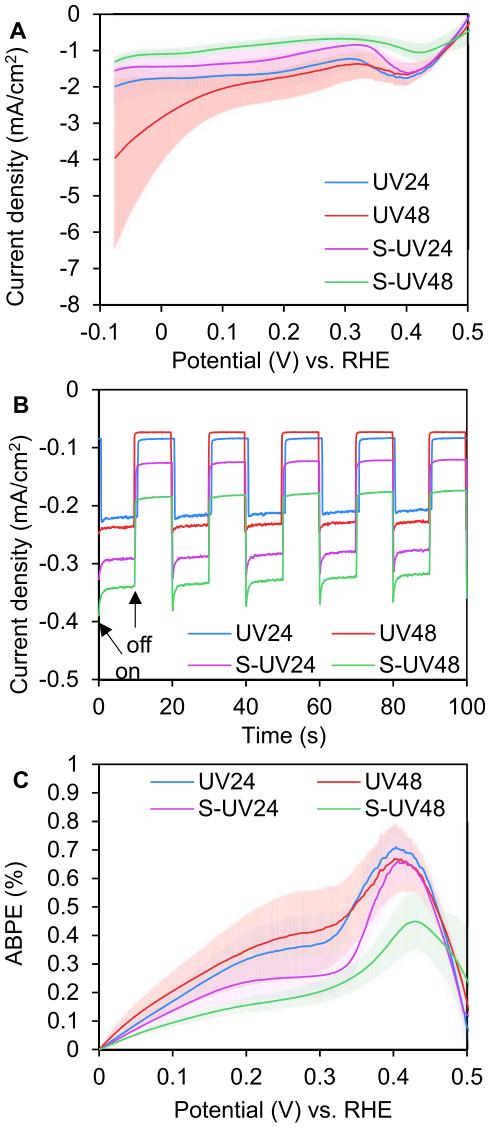

Fig. 5. Photoelectrochemical properties of the ZnO/CuO NFRs. (A) Photocurrent density vs. applied potential (J–V) curves under light illumination (100 mW/cm^2). (B) Photocurrent density vs. time (J–t) curves measured in a three-electrode setup (WE: ZnO/CuO NFRs, CE: Pt, RE: Ag/AgCl) at 0.02 V vs. RHE under intermittent light illumination (400–600 nm; 10 s light on/10 s light off). (C) Changes in the calculated applied bias photon-to-current efficiency (ABPE) as a function of the applied potential in the three-electrode setup.

Table 2
Comparison of the photocurrent densities generated in this study and previous works.

Samples	Current density	Fabrication method	Ref.
Hierarchically branched ZnO/CuO thin film	0.5 mA/cm^2 at − 0.4 V vs. Ag/AgCl	Hydrothermal method	[5]
ZnO/CuO Heterojunction Branched Nanowires	− 0.65 mA/cm^2 at − 0.45 V vs. Ag/AgCl	Hydrothermal method	[8]
ZnO nanoparticle-loaded CuO dandelion heterostructures	− 0.06 mA/cm^2 at − 0.5 V vs. Ag/AgCl	Thermal oxidation	[19]
CuO/ZnO core/shell heterostructure nanowire arrays	− 0.4 mA/cm^2 at − 0.2 V vs. SCE	Thermal oxidation	[20]
ZnO/CuO NFRs	− 2.9 mA/cm^2 at 0 V vs. RHE	G-SPSC	This study

impact.

3.4. PEC H_2 production by the ZnO/CuO NFRs

The H_2 concentration in the electrolyte was measured directly using a H_2 sensor at 0 V vs. RHE under visible-light irradiation. UV48 showed greater continuous H_2 generation over time under light irradiation than under dark conditions (Fig. 6). The slope of H_2 production slowed over time, indicating that the performance of the ZnO/CuO NFRs gradually deteriorated under visible-light irradiation. Light irradiation enhanced the H_2 generation rates of all ZnO/CuO NFRs, especially those samples subjected to longer UV irradiation, such as UV48 (Fig. 7 A). These findings indicate that the NFRs may potentially serve as semiconductor photoelectrodes. The H_2 generation rate of UV48 was 0.63 ± 0.29 μmol/cm^2/day, similar to those of S-UV24 and S-UV48. Longer UV irradiations without ZnO sputtering improved the H_2 generation rate by 2.8 times. ZnO sputtering did not improve the H_2 generation rate of UV48. These results suggest that sputtering enhances the growth speed of ZnO NRs but does not affect the total amount of ZnO NRs formed. Sputtering has been thought to be an important step in the fabrication process because it provides a ZnO seeding layer for nanostructure construction [6,8,11,36]. However, this process is complicated and energy- and time-consuming, and the electrode area that can be sputtered in a single run is greatly limited. If the ZnO sputtering could be omitted, the G-SPSC process would be more environmentally friendly and applicable to large scale fabrication of metal oxides.

The faradaic efficiencies obtained at 0 V vs. RHE under light irradiation were in the range of 0.09–0.41%, which are significantly lower than those observed at − 0.69 V vs. RHE (48.1–77.6%) (Fig. 7B). We hypothesized that this finding could be attributed to the high charge transfer resistance (R_{ct}) of the ZnO/CuO NFRs.

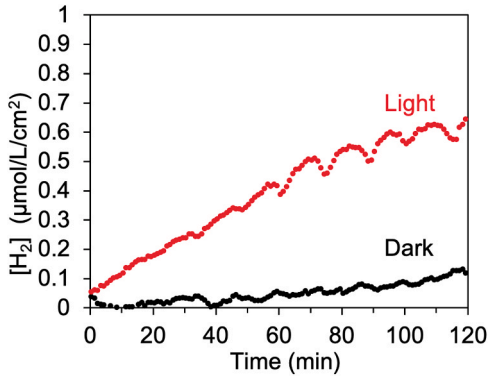

Fig. 6. Representative hydrogen generation of UV48 under light-irradiation and dark conditions at 0 V vs. RHE.

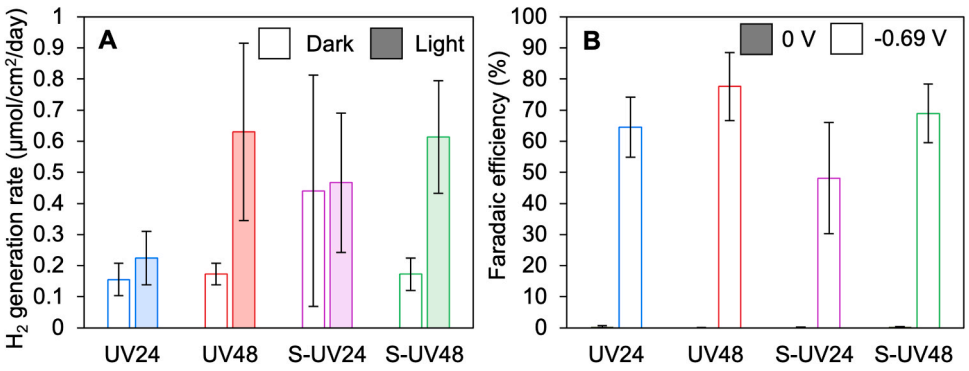

Fig. 7. (A) Photoelectrochemical (PEC) H_2 generation rate of the ZnO/CuO NFRs under light illumination (~100 mW/cm^2) with filter transmission from 400 to 600 nm and the potential maintained at 0 V vs. RHE in a three-electrode setup (WE: ZnO/CuO NFRs, CE: Pt, RE: Ag/AgCl). (B) Faradaic efficiency of the ZnO/CuO NFRs maintained at 0 V and − 0.69 V vs. RHE under light intensities of ~100 and ~230 mW/cm^2, respectively.

3.5. Charge transfer resistance of the ZnO/CuO NFRs

The R_{ct} of the ZnO/CuO NFRs was measured using EIS to examine their applicability as photocathodes for PEC or MPEC cells. EIS was performed at 0.02 V vs. RHE under light irradiation, and the results were compared with those of graphite felt, which is often used as a cathode for microbial electrochemical cells. The arc radius of the ZnO/CuO NFRs was much larger than that of the graphite felt, indicating that the R_{ct} of the former was larger than that of the latter (Fig. S3). To quantify R_{ct}, we curve-fitted the Nyquist plots of graphite felt and ZnO/CuO NFRs using pyZwx [38]. The R_{ct} of the ZnO/CuO NFRs and graphite felt were determined to be 35.6 ± 4.66 and 1.11 ± 0.07 Ω/cm^2, respectively. The R_{ct} of the ZnO/CuO NFRs was 33 times higher than that of graphite felt. The larger R_{ct2} of the ZnO/CuO NFRs requires a larger voltage to pass the same number of electrons to an electron acceptor [42], resulting in a larger overpotential. Lower activation loss can be achieved by increasing the electrode surface area, improving electrode catalysis, and increasing the operating temperature [43].

3.6. Toxicity of the ZnO/CuO NFRs to microorganisms

The potential applicability of the ZnO/CuO NFRs as photocathodes for microbial PEC (MPEC) cells was evaluated by assessing their influence on the growth of *E. coli* MG1655 (Fig. 8A). The growth of *E. coli* MG1655 was significantly inhibited when the ZnO/CuO NFRs were immersed in the growth medium (LB medium), regardless of the presence or absence of light irradiation. The maximum biomass concentration decreased by 54% in cultures without light irradiation and by 58% in cultures with light irradiation. When the potential of the ZnO/CuO NFRs was maintained at 0.01 V vs. RHE, growth inhibition was not observed with or without light irradiation as compared with the control (*E. coli*). Growth under light irradiation at 0.01 V vs. RHE was slightly higher than that under dark conditions and the control, which was probably due to the increase in temperature of the growth medium induced by light irradiation. Based on these results, we hypothesized that Zn^{2+} and Cu^{2+} could be eluted from the ZnO/CuO NFRs in the absence of potential and that these ions may inhibit the growth of *E. coli* MG1655.

To test this hypothesis, we determined the concentrations of Cu and Zn in the growth medium using ICPE. The Cu concentrations gradually

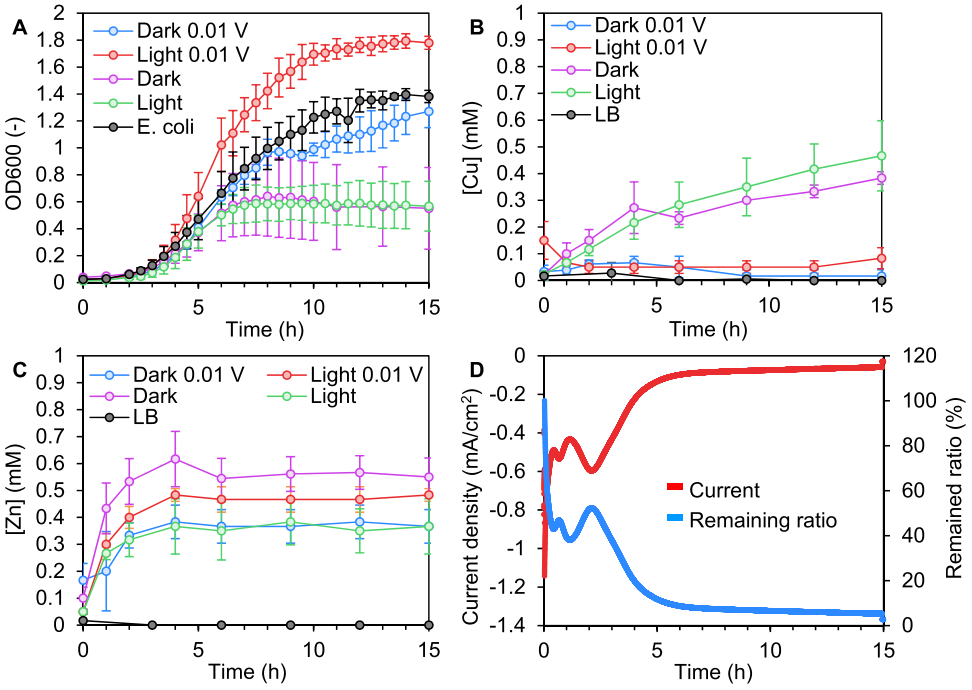

Fig. 8. (A) Effect of the nanostructured ZnO/CuO NFRs (UV48) on the growth of *E. coli* MG1655 in LB medium with 1 g/L glucose and 0.5% (v/v) DMSO. The potential of the ZnO/CuO NFRs was maintained at 0.01 V vs. RHE using a three-electrode system (WE: ZnO/CuO NFRs, CE: Pt, RE: Ag/AgCl). Each experiment was performed in triplicate except for UV48 (dark at 0.01 V vs. RHE, n = 2). (B) Cu and (C) Zn concentrations in the LB medium. (D) Photocurrent density and its remaining ratio to evaluate the photostability of the ZnO/CuO NFRs at 0.01 V vs. RHE.

increased to 0.47 ± 0.13 and 0.38 ± 0.02 mM with and without light irradiation, respectively, during 15 h of submersion in the absence of a potential (Fig. 8B). When a potential of 0.01 V vs. RHE was applied, no significant increase in Cu concentration was observed. The concentration of Zn increased and peaked in the first 4 h of the experiment and did not change thereafter, regardless of the application of potential and light irradiation (Fig. 8 C). This finding suggests that the initial increase in Zn concentration is due to the introduction of $Zn(OH)_2$, an intermediate product of G-SPSC [32] associated with the ZnO/CuO NFRs. Cu elution probably occurred because of crevice corrosion. Oxic and anoxic microenvironments were created at the top and root regions of the CuO NWs [44], acting as local cathodes and anodes, respectively. The CuO NW mesh (root region) was not coated with ZnO because ZnO sputter deposition was not applied in this experiment; however, the top region was coated with ZnO NRs. Thus, the root CuO region functioned as an anode, resulting in Cu dissolution.

In the literature, the half maximal (50%) inhibitory concentrations (IC_{50}) of Cu^{2+} for *E. coli* (ATCC 25922) have been reported to be in the range of 0.28–0.88 mM [45]. In addition, the IC_{50} of Zn^{2+} for *E. coli* (ATCC 25922) has been reported at 0.81 mM [46]. Therefore, growth inhibition can be explained by the dissolution of Cu^{2+} but not Zn^{2+}. Taking these results together, growth inhibition could be caused by Cu^{2+} dissolution, which was prevented by maintaining the potential of the ZnO/CuO NFRs at 0.01 V vs. RHE. In addition, physical contact with the ZnO/CuO NFRs (at 0.01 V vs. RHE) did not affect the growth of *E. coli* MG1655.

The current density and electrode potential during the Cu and Zn elution experiments under light irradiation were measured to evaluate the stability of the ZnO/CuO NFRs at 0.01 V vs. RHE (Fig. 8D). Initially, the current density was unstable and decreased sharply because of the high charge current of the electric double layer. The maximum current density decreased to 50% after 13 min, and approximately 50% photostability was maintained until 156 min. Subsequently, the current density decreased to approximately − 0.1 mA/cm^2 after 6 h. This stability is comparable to or superior to that of previously reported ZnO-based photocathodes, except for the photocathode with a TiO_2 protective layer (Table 3). Given that the provisional target for stability in laboratory experiments is 200 h [47], the stability of the ZnO/CuO NFRs must be further improved.

Table 3
Comparison of the stability of ZnO-based photocathodes.

Samples	Stability	Potential	Ref.
Cu_2O/ZnO photocathode	20 min, 5%	0 V vs. RHE	[48]
Cauliflower-shaped p-n CuO/ZnO heterojunction photocathodes	600 s	− 0.3 V vs. Ag/AgCl	[49]
CuO nanorod photocathode with a ZnO nanobranch protective layer	200 s	− 0.5 V vs. Ag/AgCl	[50]
CuO/ZnO/TiO_2 photocathodes	800 s, 70.8%	− 0.5 V vs. Ag/AgCl	[51]
ZnO/CuO NFRs	156 min, 45.0%	0.01 V vs. RHE	This study

4. Conclusion

We successfully synthesized high-PEC performance 3D heterostructured ZnO/CuO NFRs via thermal oxidation and UV irradiation in pure water at ambient temperature and pressure. A longer UV irradiation time significantly improved photocurrent generation in the ZnO/CuO NFRs owing to their high light absorption, large BET specific surface area, and low charge recombination. ZnO sputtering was unnecessary. Among the prepared samples, the ZnO/CuO NFRs fabricated with 48 h of UV irradiation without sputter deposition exhibited the highest photocurrent density of − 2.9 ± 1.3 mA/cm^2 and H_2 generation rate of 0.63 ± 0.29 μmol/cm^2/day at 0 V vs. RHE. The ZnO/CuO NFRs leached Cu^{2+} with or without light irradiation and inhibited the growth of *E. coli* MG1655; however, such leaching could be prevented by applying a voltage of 0.01 V vs. RHE. The results indicate that the ZnO/CuO NFRs can be used as a photocathode in PEC cells for H_2 production or MPEC systems for the synthesis of valuable CO_2-reduced products using microorganisms as catalysts as long as the potential of the NFRs is regulated at < 0.01 V vs. RHE.

CRediT authorship contribution statement

Ryosuke Matsuo: Investigation, Data curation, Writing – original draft, Funding acquisition. **Yuki Takahashi:** Supervision, Methodology. **Seiichi Watanabe:** Supervision, Methodology, Writing – review & editing, Funding acquisition. **Satoshi Okabe:** Conceptualization, Methodology, Supervision, Writing – review & editing, Funding acquisition.

Declaration of Competing Interest

The authors declare that they have no known competing financial interests or personal relationships that could have appeared to influence the work reported in this paper.

Data availability

Data will be made available on request.

Acknowledgment

We thank the Open Facility, Global Facility Center, Creative Research Institution, Hokkaido University, for allowing us to conduct the analysis of the Cu mesh, CuO NW mesh, and ZnO/CuO NFRs using Autosorb 6AG for BET specific surface area measurements and for providing insights and expertise that greatly assisted this research. XPS analysis using a JPS-9200 was conducted at the Laboratory of XPS Analysis, Joint-use Facilities, Hokkaido University. FE-SEM observations were conducted at the High-Voltage Electron Microscope Laboratory of Hokkaido University. This work was financially supported by JSPS KAKENHI 20K20486, 22K18296, and 23H00192, which were granted to Satoshi Okabe; JPMJSP2119 and JSPS KAKENHI 22J10900, and 22KJ0061, which were granted to Ryosuke Matsuo; and JSPS KAKENHI 20H00295, which were granted to Seiichi Watanabe. This study was conducted in Hokkaido University and partly supported by "Advanced Research Infrastructure for Materials and Nanotechnology in Japan (ARIM)" of the Ministry of Education, Culture, Sports, Science and Technology (MEXT).

Appendix A. Supporting information

Supplementary data associated with this article can be found in the online version at doi:10.1016/j.apcatb.2023.123097.

References

[1] N. Kornienko, J.Z. Zhang, K.K. Sakimoto, P. Yang, E. Reisner, Interfacing nature's catalytic machinery with synthetic materials for semi-artificial photosynthesis, Nat. Nanotechnol. 13 (2018) 890–899, https://doi.org/10.1038/s41565-018-0251-7.
[2] X. Fang, S. Kalathil, E. Reisner, Semi-biological approaches to solar-to-chemical conversion, Chem. Soc. Rev. 49 (2020) 4926–4952, https://doi.org/10.1039/c9cs00496c.
[3] S. Cho, J.W. Jang, K.H. Lee, J.S. Lee, Research update: Strategies for efficient photoelectrochemical water splitting using metal oxide photoanodes, APL Mater. 2 (2014), 010703, https://doi.org/10.1063/1.4861798.
[4] Y. Yang, S. Niu, D. Han, T. Liu, G. Wang, Y. Li, Progress in developing metal oxide nanomaterials for photoelectrochemical water splitting, Adv. Energy Mater. 7 (2017) 1–26, https://doi.org/10.1002/aenm.201700555.
[5] J. Wang, W. De Zhang, W.X. Ouyang, Y.X. Yu, Hierarchically branched ZnO/CuO thin film with enhanced visible light photoelectrochemical property, Mater. Lett. 154 (2015) 44–46, https://doi.org/10.1016/j.matlet.2015.04.048.

[6] A. Kargar, K. Sun, Y. Jing, C. Choi, H. Jeong, G.Y. Jung, S. Jin, D. Wang, 3D Branched nanowire photoelectrochemical electrodes for efficient solar water splitting, ACS Nano 7 (2013) 9407–9415, https://doi.org/10.1021/nn404170y.

[7] I.S. Cho, Z. Chen, A.J. Forman, D.R. Kim, P.M. Rao, T.F. Jaramillo, X. Zheng, Branched TiO_2 nanorods for photoelectrochemical hydrogen production, Nano Lett. 11 (2011) 4978–4984, https://doi.org/10.1021/nl2029392.

[8] A. Kargar, Y. Jing, S.J. Kim, C.T. Riley, X. Pan, D. Wang, ZnO/CuO heterojunction branched nanowires for photoelectrochemical hydrogen generation, ACS Nano 7 (2013) 11112–11120, https://doi.org/10.1021/nn404838n.

[9] K. Sun, Y. Jing, C. Li, X. Zhang, R. Aguinaldo, A. Kargar, K. Madsen, K. Banu, Y. Zhou, Y. Bando, Z. Liu, D. Wang, 3D branched nanowire heterojunction photoelectrodes for high-efficiency solar water splitting and H_2 generation, Nanoscale 4 (2012) 1515–1521, https://doi.org/10.1039/c2nr11952h.

[10] J. Lee, K. Yong, Combining the lotus leaf effect with artificial photosynthesis: Regeneration of underwater superhydrophobicity of hierarchical ZnO/Si surfaces by solar water splitting, NPG Asia Mater. 7 (2015), e201, https://doi.org/10.1038/am.2015.74.

[11] A. Kargar, K. Sun, Y. Jing, C. Choi, H. Jeong, Y. Zhou, K. Madsen, P. Naughton, S. Jin, G.Y. Jung, D. Wang, Tailoring n-ZnO/p-Si branched nanowire heterostructures for selective photoelectrochemical water oxidation or reduction, Nano Lett. 13 (2013) 3017–3022, https://doi.org/10.1021/nl304539x.

[12] Y.X. Yu, W.X. Ouyang, Z.T. Liao, B. Bin Du, W. De Zhang, Construction of ZnO/ZnS/CdS/$CuInS_2$ core-shell nanowire arrays via ion exchange: P-n junction photoanode with enhanced photoelectrochemical activity under visible light, ACS Appl. Mater. Interfaces 6 (2014) 8467–8474, https://doi.org/10.1021/am501336u.

[13] J. Li, F. Meng, S. Suri, W. Ding, F. Huang, N. Wu, Photoelectrochemical performance enhanced by a nickel oxide-hematite p-n junction photoanode, Chem. Commun. 48 (2012) 8213–8215, https://doi.org/10.1039/c2cc30376k.

[14] K.S. Ahn, Y. Yan, S. Shet, K. Jones, T. Deutsch, J. Turner, M. Al-Jassim, ZnO nanocoral structures for photoelectrochemical cells, Appl. Phys. Lett. 93 (2008) 98–101, https://doi.org/10.1063/1.3002282.

[15] K.S. Ahn, S. Shet, T. Deutsch, C.S. Jiang, Y. Yan, M. Al-Jassim, J. Turner, Enhancement of photoelectrochemical response by aligned nanorods in ZnO thin films, J. Power Sources 176 (2008) 387–392, https://doi.org/10.1016/j.jpowsour.2007.10.034.

[16] Y.F. Lim, C.S. Chua, C.J.J. Lee, D. Chi, Sol-gel deposited Cu_2O and CuO thin films for photocatalytic water splitting, Phys. Chem. Chem. Phys. 16 (2014) 25928–25934, https://doi.org/10.1039/c4cp03241a.

[17] S. Masudy-Panah, R. Siavash Moakhar, C.S. Chua, H.R. Tan, T.I. Wong, D. Chi, G. K. Dalapati, Nanocrystal engineering of sputter-grown CuO photocathode for visible-light-driven electrochemical water splitting, ACS Appl. Mater. Interfaces 8 (2016) 1206–1213, https://doi.org/10.1021/acsami.5b09613.

[18] T. Chang, Z. Li, G. Yun, Y. Jia, H. Yang, Enhanced photocatalytic activity of ZnO/CuO nanocomposites synthesized by hydrothermal method, Nano-Micro Lett. 5 (2013) 163–168, https://doi.org/10.5101/nml.v5i3.p163-168.

[19] G. Dong, B. Du, L. Liu, W. Zhang, Y. Liang, H. Shi, W. Wang, Synthesis and their enhanced photoelectrochemical performance of ZnO nanoparticle-loaded CuO dandelion heterostructures under solar light, Appl. Surf. Sci. 399 (2017) 86–94, https://doi.org/10.1016/j.apsusc.2016.12.024.

[20] X. Zhao, P. Wang, B. Li, CuO/ZnO core/shell heterostructure nanowire arrays: Synthesis, optical property, and energy application, Chem. Commun. 46 (2010) 6768–6770, https://doi.org/10.1039/c0cc01610a.

[21] Z. Liu, H. Bai, S. Xu, D.D. Sun, Hierarchical CuO/ZnO “corn-like” architecture for photocatalytic hydrogen generation, Int. J. Hydrog. Energy 36 (2011) 13473–13480, https://doi.org/10.1016/j.ijhydene.2011.07.137.

[22] C. Zhou, L. Xu, J. Song, R. Xing, S. Xu, D. Liu, H. Song, Ultrasensitive non-enzymatic glucose sensor based on three-dimensional network of ZnO-CuO hierarchical nanocomposites by electrospinning, Sci. Rep. 4 (2014) 1–9, https://doi.org/10.1038/srep07382.

[23] T. Soejima, K. Takada, S. Ito, Alkaline vapor oxidation synthesis and electrocatalytic activity toward glucose oxidation of CuO/ZnO composite nanoarrays, Appl. Surf. Sci. 277 (2013) 192–200, https://doi.org/10.1016/j.apsusc.2013.04.024.

[24] A. Zainelabdin, G. Amin, S. Zaman, O. Nur, J. Lu, L. Hultman, M. Willander, CuO/ZnO Nanocorals synthesis via hydrothermal technique: Growth mechanism and their application as Humidity Sensor, J. Mater. Chem. 22 (2012) 11583–11590, https://doi.org/10.1039/c2jm16597j.

[25] B. Li, Y. Wang, Facile synthesis and photocatalytic activity of ZnO-CuO nanocomposite, Superlattices Micro 47 (2010) 615–623, https://doi.org/10.1016/j.spmi.2010.02.005.

[26] A. Lavín, R. Sivasamy, E. Mosquera, M.J. Morel, High proportion ZnO/CuO nanocomposites: Synthesis, structural and optical properties, and their photocatalytic behavior, Surf. Interfaces 17 (2019), 100367, https://doi.org/10.1016/j.surfin.2019.100367.

[27] Q. Simon, D. Barreca, A. Gasparotto, C. MacCato, T. Montini, V. Gombac, P. Fornasiero, O.I. Lebedev, S. Turner, G. Van Tendeloo, Vertically oriented CuO/ZnO nanorod arrays: From plasma-assisted synthesis to photocatalytic H_2 production, J. Mater. Chem. 22 (2012) 11739–11747, https://doi.org/10.1039/c2jm31589k.

[28] Z.L. Liu, J.C. Deng, J.J. Deng, F.F. Li, Fabrication and photocatalysis of CuO/ZnO nano-composites via a new method, Mater. Sci. Eng. B Solid-State Mater. Adv. Technol. 150 (2008) 99–104, https://doi.org/10.1016/j.mseb.2008.04.002.

[29] X.M. Song, C. Yuan, Y. Wang, B. Wang, H. Mao, S. Wu, Y. Zhang, ZnO/CuO photoelectrode with n-p heterogeneous structure for photoelectrocatalytic oxidation of formaldehyde, Appl. Surf. Sci. 455 (2018) 181–186, https://doi.org/10.1016/j.apsusc.2018.05.196.

[30] C. Liu, F. Meng, L. Zhang, D. Zhang, S. Wei, K. Qi, J. Fan, H. Zhang, X. Cui, CuO/ZnO heterojunction nanoarrays for enhanced photoelectrochemical water oxidation, Appl. Surf. Sci. 469 (2019) 276–282, https://doi.org/10.1016/j.apsusc.2018.11.054.

[31] Z. Guo, X. Chen, J. Li, J.H. Liu, X.J. Huang, ZnO/CuO hetero-hierarchical nanotrees array: Hydrothermal preparation and self-cleaning properties, Langmuir 27 (2011) 6193–6200, https://doi.org/10.1021/la104979x.

[32] Y. Takahashi, K. Hiraiwa, M. Jeem, L. Zhang, S. Watanabe, Galvanic-submerged photosynthesis of crystallites: Fabrication of ZnO nanorods@ Cu-surface, Appl. Surf. Sci. 489 (2019) 313–320, https://doi.org/10.1016/j.apsusc.2019.05.348.

[33] K. Hiraiwa, Y. Takahashi, J. Mizuno, M. Jeem, S. Watanabe, Luminescence properties of ZnO-M heterostructures fabricated by galvanic-submerged photosynthesis of crystallites, Appl. Surf. Sci. 489 (2019) 269–277, https://doi.org/10.1016/j.apsusc.2019.05.292.

[34] M. Jeem, M.R.M. Bin Julaihi, J. Ishioka, S. Yatsu, K. Okamoto, T. Shibayama, T. Iwasaki, T. Kato, S. Watanabe, A pathway of nanocrystallite fabrication by photo-assisted growth in pure water, Sci. Rep. 5 (2015) 1–9, https://doi.org/10.1038/srep11429.

[35] L. Zhang, M. Jeem, K. Okamoto, S. Watanabe, Photochemistry and the role of light during the submerged photosynthesis of zinc oxide nanorods, Sci. Rep. 8 (2018) 1–13, https://doi.org/10.1038/s41598-017-18572-8.

[36] Y. Takahashi, M. Jeem, L. Zhang, S. Watanabe, The origin of opto-functional enhancement in ZnO/CuO nanoforest structure fabricated by submerged photosynthesis, Appl. Mater. Today 26 (2022), 101359, https://doi.org/10.1016/j.apmt.2021.101359.

[37] A.M.B. Goņalves, L.C. Campos, A.S. Ferlauto, R.G. Lacerda, On the growth and electrical characterization of CuO nanowires by thermal oxidation, J. Appl. Phys. 106 (2009), 034303, https://doi.org/10.1063/1.3187833.

[38] K. Kobayashi, T.S. Suzuki, Free analysis and visualization programs for electrochemical impedance spectroscopy coded in python, Electrochemistry 89 (2021) 218–222, https://doi.org/10.5796/electrochemistry.21-00010.

[39] M. Jeem, L. Zhang, J. Ishioka, T. Shibayama, T. Iwasaki, T. Kato, S. Watanabe, Tuning Optoelectrical Properties of ZnO Nanorods with Excitonic Defects via Submerged Illumination, Nano Lett. 17 (2017) 2088–2093, https://doi.org/10.1021/acs.nanolett.7b00324.

[40] J.Y. Zheng, G. Song, C.W. Kim, Y.S. Kang, Facile preparation of p-CuO and p-CuO/n-$CuWO_4$ junction thin films and their photoelectrochemical properties, Electrochim. Acta 69 (2012) 340–344, https://doi.org/10.1016/j.electacta.2012.03.011.

[41] J. Han, H. Xing, Q. Song, H. Yan, J. Kang, Y. Guo, Z. Liu, A ZnO@CuO core-shell heterojunction photoanode modified with ZnFe-LDH for efficient and stable photoelectrochemical performance, Dalt. Trans. 50 (2021) 4593–4603, https://doi.org/10.1039/d1dt00336d.

[42] N. Tian, H. Huang, C. Liu, F. Dong, T. Zhang, X. Du, S. Yu, Y. Zhang, *In situ* co-pyrolysis fabrication of CeO_2/g-C_3N_4 n-n type heterojunction for synchronously promoting photo-induced oxidation and reduction properties, J. Mater. Chem. A 3 (2015) 17120–17129, https://doi.org/10.1039/c5ta03669k.

[43] W.V, K.R, Bruce E. Logan, Hamelers Bert, Rozendal René, Shroder Uwe, Keller Jurg, Freguia Stefano, Aelterman Peter, Critical Review Microbial Fuel Cells: Methodology and Technology, Environ. Sci. Technol. 40 (2006) 5181–5192, http://pubs.acs.org/doi/abs/10.1021/es0605016.

[44] C. Liu, J.J. Gallagher, K.K. Sakimoto, E.M. Nichols, C.J. Chang, M.C.Y. Chang, P. Yang, Nanowire-bacteria hybrids for unassisted solar carbon dioxide fixation to value-added chemicals, Nano Lett. 15 (2015) 3634–3639, https://doi.org/10.1021/acs.nanolett.5b01254.

[45] C. Kaweeteerawat, C.H. Chang, K.R. Roy, R. Liu, R. Li, D. Toso, H. Fischer, A. Ivask, Z. Ji, J.I. Zink, Z.H. Zhou, G.F. Chanfreau, D. Telesca, Y. Cohen, P.A. Holden, A. E. Nel, H.A. Godwin, Cu Nanoparticles Have Different Impacts in *Escherichia coli* and *Lactobacillus brevis* than Their Microsized and Ionic Analogues, ACS Nano 9 (2015) 7215–7225, https://doi.org/10.1021/acsnano.5b02021.

[46] D. Fang, G. Gao, J. Shen, Y. Yu, J. Zhi, A reagentless electrochemical biosensor based on thionine wrapped *E. coli* and chitosan-entrapped carbon nanodots film modified glassy carbon electrode for wastewater toxicity assessment, Electrochim. Acta 222 (2016) 303–311, https://doi.org/10.1016/j.electacta.2016.10.174.

[47] Z. Chen, T.F. Jaramillo, T.G. Deutsch, A. Kleiman-Shwarsctein, A.J. Forman, N. Gaillard, R. Garland, K. Takanabe, C. Heske, M. Sunkara, E.W. McFarland, K. Domen, E.L. Milled, H.N. Dinh, Accelerating materials development for photoelectrochemical hydrogen production: Standards for methods, definitions, and reporting protocols, J. Mater. Res 25 (2010) 3–16, https://doi.org/10.1557/jmr.2010.0020.

[48] L. Diao, L. Zheng, R. Zhang, F. Chen, Y. Li, W. Wang, F. Lu, L. Chen, H. Liu, H. Dong, Y. Cheng, Titanium Nitride Protected Cuprous Oxide Photocathode for Stable and Efficient Water Reduction, ACS Appl. Energy Mater. 5 (2022) 770–776, https://doi.org/10.1021/acsaem.1c03240.

[49] K. Zhang, W.F. Cai, J.W. Shi, Q.Y. Chen, Architecture lattice-matched cauliflower-like CuO/ZnO p–n heterojunction toward efficient water splitting, J. Chem. Technol. Biotechnol. 97 (2022) 914–923, https://doi.org/10.1002/jctb.6974.

[50] U. Shaislamov, K. Krishnamoorthy, S.J. Kim, W. Chun, H.J. Lee, Facile fabrication and photoelectrochemical properties of a CuO nanorod photocathode with a ZnO nanobranch protective layer, RSC Adv. 6 (2016) 103049–103056, https://doi.org/10.1039/c6ra18832j.

[51] U. Shaislamov, H. Kim, J.M. Yang, B.L. Yang, CuO/ZnO/TiO_2 photocathodes for a self-sustaining photocell: Efficient solar energy conversion without external bias

and under visible light, Int. J. Hydrog. Energy 45 (2020) 6148–6158, https://doi.org/10.1016/j.ijhydene.2019.12.052.